
Article:
Hu, Y, He, Y, Zhang, Z et al. (1 more author) (2019) Enhanced heat capacity of binary nitrate eutectic salt-silica nanofluid for solar energy storage. Solar Energy Materials and Solar Cells, 192. pp. 94-102. ISSN 0927-0248

https://doi.org/10.1016/j.solmat.2018.12.019

Enhanced heat capacity of binary nitrate eutectic salt-silica nanofluid for solar energy storage

Yanwei Hu[1], Yurong He[1]*, Zhenduo Zhang[1], Dongsheng Wen[2, 3]

1, School of Energy Science & Engineering, Harbin Institute of Technology, Harbin, China, 150001

2, School of Aeronautic Science and Engineering, Beihang University, Beijing, China, 100191

3, School of Chemical and Process Engineering, University of Leeds, Leeds, U.K., LS2 9JT

*Corresponding author. E-mail address: rong@hit.edu.cn

Abstract: In concentrating solar power plants, the heat capacity of thermal storage media is a key factor that affects the cost of electricity generation. This work investigated the effective specific heat capacity of binary nitrate eutectic salts seeded with silica nanoparticles, using both experimental measurements and molecular dynamics simulations. The effects of the mass concentration (0–2.0 wt.%) and average size (10, 20, and 30 nm) of the nanoparticles on the specific heat capacity value of nanofluids were analyzed. The results show that specific heat capacity increases when adding 10 nm silica nanoparticles up to 1.0 wt.%, and then it decreases at higher concentrations. At this optimal mass concentration, the 20 nm nanoparticles displayed a maximum enhancement in the average specific heat capacity (by ~26.7%). The simulation results provided information about the different energy components in the system. The rate of potential energy change versus nanoparticle mass concentration was found to be maximized at 1.0 wt.% concentration, which agrees with the experimental measurements. The potential energy components in the simulation system indicate that the change of Coulombic energy contributes the most to the variation of specific heat capacity.

Keywords: solar energy storage; molten salt based nanofluids; specific heat capacity; molecular dynamics simulation

1. Introduction

Solar energy has long been regarded as one of the main energy sources for the future, due to its virtually unlimited amount and environmentally friendly nature. Thermal energy storage systems play a vital role in the utilization of solar energy, by reducing the mismatch between energy supply and demand and therefore improving the performance and reliability of electricity production by harnessing solar thermal

energy. Due to their low vapor pressure, high latent heat, and wide operating temperature range [1], molten salts are widely used in these thermal storage systems, such as at the Andasol, Valle, and Themis solar power stations and Archimede solar power plant [2,3]. However, the thermophysical properties of molten salts used in these systems are not ideal, with their specific heat capacities less than 1.6 kJ/(kg·K) and thermal conductivities less than 1.0 W/(m·K) [4]. Considering the large amount of heat transfer fluid (HTF) and thermal energy storage (TES) materials required in a concentrating solar power (CSP) plant, it is necessary to reduce their cost while enhancing their heat transfer and thermal storage performance. Many researchers have focused on the study, design, and characterization of salts to develop thermal storage materials with improved properties [5–7].

Seeding nanoparticles with excellent thermal properties can effectively improve the thermal conductivity and associated convective heat transfer [8–12]. Recently, the effect of nanoparticles on specific heat capacity has been investigated, especially for salt- and ionic liquid-based nanofluids [13]. Shin and Banerjee [14,15] measured the specific heat capacity of eutectic salt based nanofluids and investigated the microstructure change of this nanofluid. Tao et al. [16] used four kinds of carbon nanomaterials with different microstructures to formulate carbonate salt based nanomaterial composite and a maximum enhancement in specific heat capacity of 18.57% was obtained. Chen et al. [17] proposed a novel method to prepare molten salt based nanofluids. During the preparation, molten salts were melting at high temperature and nanoparticles were dispersed in molten salt by magnetic stirring. The specific heat capacity enhancement was 16.4%, compared with that of pure molten salt. Luo et al. [18] used a one-step method to synthesize molten salt based CuO nanofluids and found a maximum increment of 11.48%. Using mechanical grinding and mixing, Ding et al. [19] obtained a 10.48% enhancement of specific heat capacity with CuO nanoparticles at the concentration of 0.1 wt.%. Zhang et al.[20] doped SiO_2 nanoparticles into a quaternary nitrate with low melting point and investigated the effect of ultra-sonication time on specific heat capacity. They finally obtained an average enhancement of 19.4% with the optimal ultra-sonication time. Jo and Banerjee [21,22] investigated the influence of carbon materials such as graphite and multi-walled carbon nanotubes in carbonate salt, and significant enhancements were obtained even with a minute amount of added nanotubes. Ho and Pan [23] studied alumina nanoparticles doped in molten HITEC, and showed that the optimal concentration was about 0.063 wt.% with a specific heat capacity enhancement of

19.9%. Sang et al. [24] investigated the effect of different nanoparticles using ternary carbonates as base fluids and found the enhancement of specific heat capacity was 79.9~113.7%. Though it is established that adding nanoparticles to molten salt can significantly enhance specific heat capacity, the enhancement ratios are very different, and the reported effects of nanoparticle size are inconsistent. For example, Seo et al. [25] and Tiznobaik et al. [26] found no significant variation in specific heat capacity with nanoparticle size, while in the investigation of Dudda et al. [27], the specific heat capacity of nanomaterials was enhanced by increasing the nanoparticle size.

To explain the enhancement of specific heat capacity, Shin et al. [14,28,29] proposed three possible mechanisms: (1) the relatively higher specific heat capacity of the nanosized particles than the base material, (2) the solid-fluid interaction energy, and (3) a high-density layer formed at the nanoparticle surface. Mechanism (1) is clearly not plausible, as most nanoparticles actually have lower specific heat capacity than the base salt, even after assuming that the heat capacity is enhanced upon forming nanoparticles. Some studies [13,30] have reviewed the influences of nanoparticles with many idealized assumptions. However, the exact reasons for the specific heat capacity enhancement remain debatable. Considering the interaction between molecules, molecular dynamics simulations (MDS) provided a powerful tool to investigate nanoscale phenomena [31,32]. Qiao et al. [33] calculated specific heat capacity using MDS, and their results show an enhanced specific heat capacity. Jo et al. [34,35] simulated the interfacial thermal resistance between carbon nanoparticles and salt molecules, and calculated the thickness of the compressed layer. However, these results are still far from clarifying the mechanism of the enhanced heat capacity.

The purposes of this work are to develop a potential thermal storage material by adding nanoparticles into binary eutectic nitrate salts, and to study the effects of silica nanoparticle concentration and size on specific heat capacity. Meanwhile, a scanning electron microscope (SEM) was employed to analyze the sample morphology after the differential scanning calorimetry (DSC) measurement, and MD simulations were carried out to calculate the specific heat capacity of the nanofluids in order to reveal the cause of its enhancement. Differing from the previous MD simulations, the current work analyzed the MD results from the perspective of energy distribution of the ensemble.

2. Experiments

2.1 Nanofluid synthesis

Sodium nitrate ($NaNO_3$) and potassium nitrate (KNO_3) were obtained from Tianjin Fengchuan Chemical Reagent Technologies Co., Ltd., both with purities above 99.0%. Amorphous silica nanoparticles were purchased from Sigma-Aldrich Co., Ltd. (10 and 20 nm) and Beijing DK Nano Technology Co., Ltd. (30 nm). Transmission Electron Microscope (TEM) was used to verify the size of SiO_2 nanoparticles Nano measure 1.2 software was used to obtain nanoparticle size distributions, as shown in Fig. 1. It can be seen that the sizes of nanoparticles were 19.4, 25.9, and 37.4 nm respectively, a little larger than those stated by manufacturer. The nanofluids were prepared based on a liquid solution method, and the main procedure is shown in Fig. 2. Initially, 4mg nanoparticles were dispersed into 20 ml of deionized water, stirred, and sonicated for 60 min in an ultrasonicator; in order to ensure good dispersion of the nanoparticles. Then, different amounts of eutectic mixture of $NaNO_3$ and KNO_3 with a mass ratio of 60:40 were dissolved in the suspension to make nanoparticle mass fraction range from 0.5% to 2.0%. The mixture was ultrasonicated for another 60 min to guarantee the uniformity and stability of the mixture. Afterwards, the solution was heated in a vacuum drying oven at 110 °C for 7 h to obtain the nanofluid without moisture. To avoid the effect of moisture, the samples were heated again before the DSC measurement.

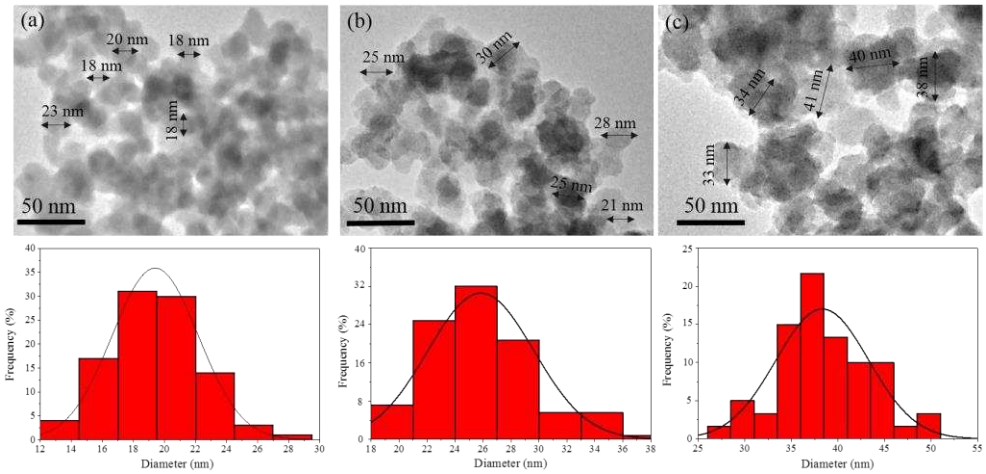

Fig. 1. TEM images and size distributions for different nanoparticles (a)10 nm (2)20 nm (3)30 nm.

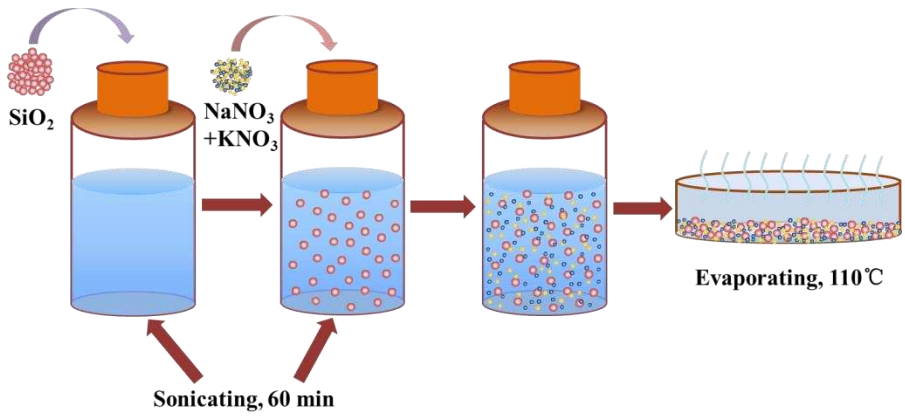

Fig. 2 Procedure of preparing the nanofluids.

2.2 Specific heat capacity measurement

The specific heat capacity of the samples was measured using DSC (204F1, NETZSCH) based on a standard test method proposed by American Society for Testing and Materials (ASTM E1269) [36]. Aluminum pans covered with pierced lids (avoiding the influence of air expansion on the shape of sealed pans) were used to hold the samples (5–15 mg, as weighed by a highly accurate electronic balance (MC 21S, Sartorius)). Before the DSC measurement, each sample was kept at 140 °C for 30 min to remove any absorbed moisture and maintained at 140 °C for another 5 min to stabilize the signal of the calorimeter. A ramping rate of 20 °C/min was employed during the measurement, and the end temperature was set to 450 °C. The sample was further maintained at 450 °C for 5 min to ensure the stability of the signal. After the measurement, the weight change was less than 0.05 mg, indicating few nanoparticles float into the air.

Initially, an experimental run was performed with an empty pan to obtain the baseline of the heat flux. Then, the heat flux of standard sapphire was measured for calibration. After that, the same procedure was repeated 3 times for each binary salt sample to ensure the reproducibility of the results and three randomly selected samples were measured for each mass fraction of nanoparticles. Since for one integrated test, it will last for more than 3 h and the samples will undergo meltdown and solidification for three times. The good repeatability for one sample can also ensure the stability of nanofluid. The morphology of the samples after DSC was examined using SEM (JSM-7500F).

The uncertainties of the experimental results depend on the measurement errors of the mass and heat flow. The specific heat capacity was determined by equation (1):

$$c_{p,s} = c_{p,sapp} \cdot \frac{\Delta q_s \cdot m_{sapp}}{\Delta q_{sapp} \cdot m_s} \tag{1}$$

where q is the heat flow and m is the sample weight. Subscripts s and sapp denote salt samples and sapphire, respectively. Then the uncertainty of the experiment can be expressed as [37]:

$$\frac{\delta c_{p,s}}{|c_{p,s}|} = \sqrt{\left(\frac{\delta q_s}{|q_s|}\right)^2 + \left(\frac{\delta q_{sapp}}{|q_{sapp}|}\right)^2 + \left(\frac{\delta m_{sapp}}{|m_{sapp}|}\right)^2 + \left(\frac{\delta m_s}{|m_s|}\right)^2} \tag{2}$$

The accuracy of the electronic balance is ±0.005 mg, and that of the heat flow is ±0.1 μW. Hence, the maximum measurement uncertainty of specific heat capacity was estimated to be 1.7%.

3. Molecular dynamics simulation

MD simulations were performed to explore the interaction between the nanoparticle and solvent molecules, using the Large-scale Atomic/Molecular Massively Parallel Simulator (LAMMPS) package [33]. A SiO_2 nanoparticle was placed at the center of the box, and the eutectic salt molecules were placed randomly in the box as shown in Fig. 3. Due to the computational limitation, the diameter of the SiO_2 nanoparticle was set as 20 Å. The concentration of the nanoparticles was adjusted from 0–2.0 wt.% by changing the length of the simulation box. Periodic boundary conditions were applied to the simulation domain.

The interaction between two non-bonded atoms was determined by a Lennard-Jones (L-J) potential with the long-range Coulomb force, as shown in equation (3) [21,38]. E(r) is the potential of the two atoms, r is their distance, q_i and q_j are the charges on atoms i and j, ε is the depth of the potential well, and σ is the finite distance at which the inter-particle potential is zero. For the interaction between different atomic species, the L-J parameters were computed by the arithmetic mean according to equation (4) [39]. A cutoff radius of 12 Å was used for calculating the L-J interactions. In addition, bond-stretching, bond-bending, and torsion were considered for the bonded interactions, as shown in equation (5). All parameters used in the MD simulation were obtained from Materials Studios and literature [40] and were listed in Table 1.

$$E(r) = \frac{q_i q_j}{r} + 4\varepsilon\left[\left(\frac{\sigma}{r}\right)^{12} - \left(\frac{\sigma}{r}\right)^{6}\right] \tag{3}$$

$$\varepsilon_{i,j} = \sqrt{\varepsilon_i \cdot \varepsilon_j}\ ,\quad \sigma_{i,j} = \frac{\left(\sigma_i + \sigma_j\right)}{2} \tag{4}$$

$$E = K_s \cdot \left(r - r_0\right)^2 + K_b \cdot \left(\theta - \theta_0\right) + K_t \cdot \left(1 + d \cdot \cos\left(n\phi\right)\right) \tag{5}$$

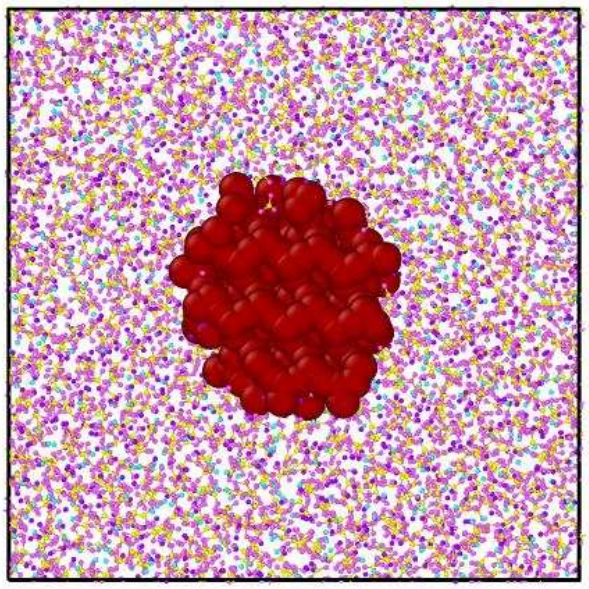

Fig. 3 Simulation domain showing a SiO_2 nanoparticle surrounded by nitrate salt molecules.

Table 1 Parameters for MD simulation.

Lennard-Jones constants				
Material	Interaction	ε[kcal/mol]	σ[Å]	Charge
SiO_2	Si-Si	0.040	4.053	+2.4
	O-O	0.228	2.860	-1.2
Eutectic	N-N	0.167	3.501	+0.95
	O-O	0.228	2.860	-0.65
	Na-Na	1.607	1.897	+1.0
	K-K	5.451	3.197	+1.0

Bonded interaction							
Material	Stretching		Bending		Improper Torsional		
	k_s	r_0	k_b	θ_0	k_i	d_i	n_i
SiO_2	392.8	1.665	42.3	113.1	26.270	-1	2
			31.1	149.8			
Eutectic	525.0	1.268	105.0	120.0	26.270	-1	2

Initially, a SiO_2 nanoparticle was located at the center of the box and the solvent molecules were placed randomly in the box. In this configuration, it is very likely for atoms to get too close to cause non-physical interactions between the particle and solvent molecules. Hence, an energy minimization step was implemented to redistribute the atoms. During this step, the temperature of the system was reduced to

0 K. Afterwards, a microcanonical ensemble was used to perform the relaxation procedure, using NVE integration (in which the number of atoms (N), the volume of the system (V), and the total energy of the system (E) were held fixed). Subsequently, the system temperature was raised to 650 K. A canonical Nose-Hoover thermostat (NVT integration, with constant N, V, and temperature (T) controlled through direct temperature scaling) was used for the temperature range from 550 to 750 K to obtain the specific heat capacity of the system in liquid phase (the melting point was about 500 K).

4. Results and discussion

4.1 Experimental results

In this study, the average specific heat capacity of the pure eutectic salt in liquid phase was found to be 1.560 J/(g·K), which is comparable with the value of 1.50–1.53 J/(g·K) in the literature [41] within 5% difference. Its melting point was up to 215 °C based on the extrapolation method, which is also similar to the literature result 220 °C [41]. To illustrate the stability of the samples, 6 thermal cycles for 1.0 wt.% nanofluids were run and the heat flux curves were shown in Fig. 4. The thermal cycles last for more than 6 h, and the heat flux curves showed good repeatability, indicating the stability of the samples. Moreover, X-ray diffraction (XRD) analysis was carried out before and after the thermal cycles, as shown in Fig. 5. It also indicates the stability of the samples.

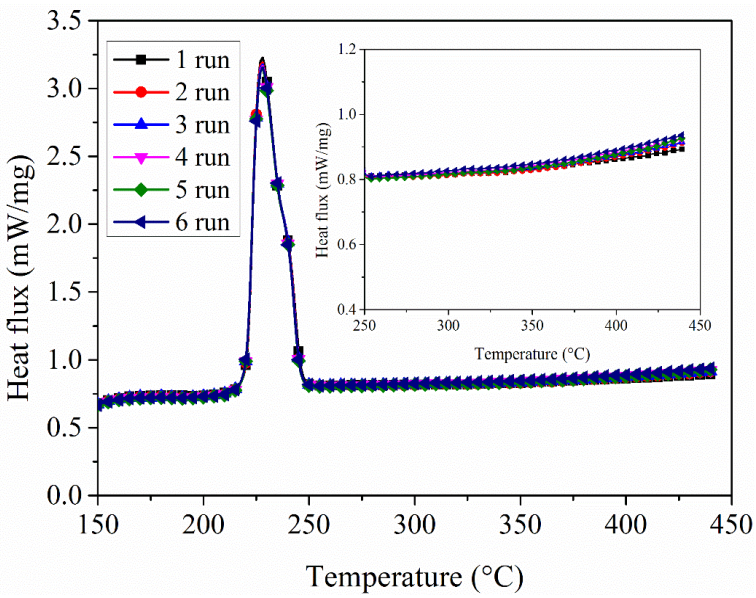

Fig. 4 Heat flux for different thermal cycles.

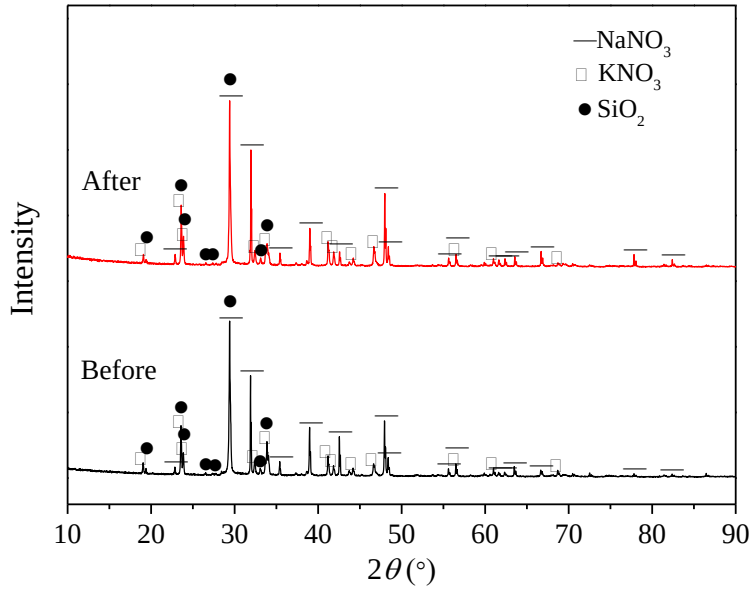

Fig. 5 XRD patterns of nanofluid before and after thermal cycles.

Fig. 6 shows the variation of specific heat capacity with temperature, for both the base salt and after seeding with nanoparticles at different mass concentrations (0.5–2.0 wt.%). The specific heat capacity of the salt containing nanoparticles at low concentrations (up to 1.0 wt.%) was higher compared to that of the base salt. Adding more nanoparticles (i.e., 1.5 wt.% and above), however, leads to a relative reduction in specific heat capacity.

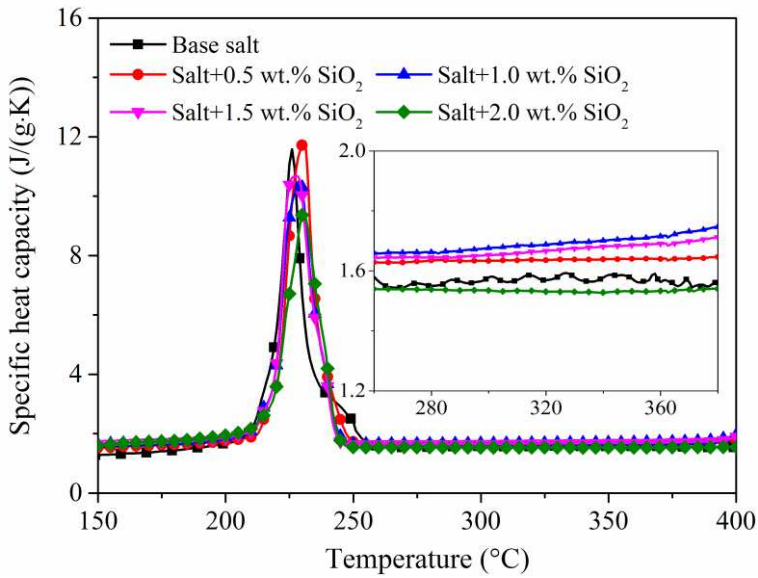

Fig. 6 Specific heat capacity vs. temperature for nanofluids with different mass fractions.

Fig. 7 gives the average specific heat capacity versus the content of nanoparticles in the liquid phase, showing that there is an optimal mass concentration (~ 1.0 wt.%) when using 10 nm SiO_2 nanoparticles to enhance the specific heat capacity of the binary nitrate eutectic salt. This is consistent with the results from Briges et al. [42]

who showed that specific heat capacity is enhanced at low nanoparticle concentrations and reduced at high concentrations. The maximum specific heat capacity enhancement is about 8.4% relative to the base salt in the present work. The specific heat capacities for each sample and each run were listed in Table 2.

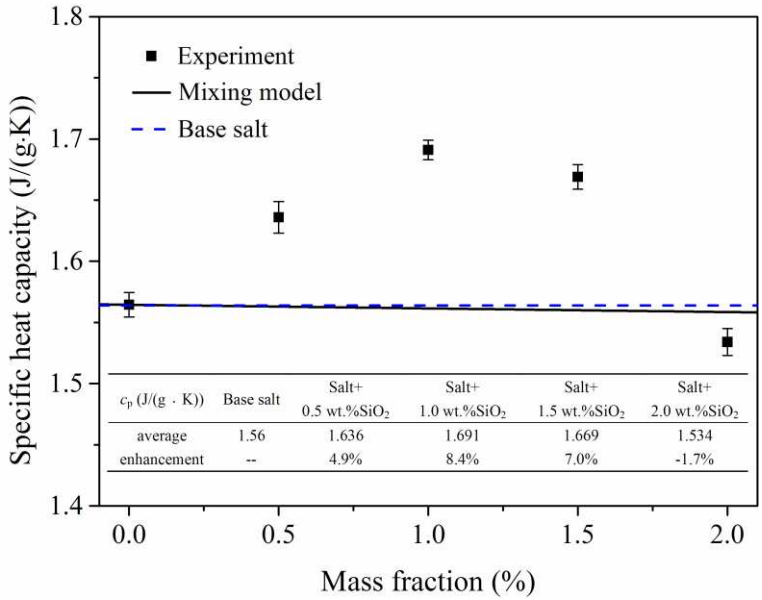

Fig. 7 Average specific heat capacity of pure base salt and after adding different amounts of 10 nm nanoparticles in the liquid phase.

Table 2 Specific heat capacities of nanofluids with different mass fractions

Sample	Base salt	Salt+ 0.5wt.%SiO_2	Salt+ 1.0wt.%SiO_2	Salt+ 1.5wt.%SiO_2	Salt+ 2.0wt.%SiO_2
1# First	1.558	1.648	1.683	1.669	1.523
1# Second	1.570	1.640	1.689	1.674	1.530
1# Third	1.563	1.645	1.685	1.675	1.528
2# First	1.563	1.633	1.697	1.667	1.534
2# Second	1.555	1.625	1.699	1.661	1.538
2# Third	1.551	1.623	1.699	1.660	1.538
3# First	1.565	1.637	1.685	1.673	1.539
3# Second	1.552	1.642	1.690	1.671	1.537
3# Third	1.562	1.632	1.691	1.670	1.539
Average	1.560	1.636	1.691	1.669	1.534
Enhancement	--	4.9%	8.4%	7.0%	-1.7%

Fig. 7 indicates that the enhancement in specific heat capacity could not be predicted by the conventional effective specific heat capacity model based on the simple mixing theory:

$$c_{p,nf} = \frac{m_{np}c_{p,np} + m_s c_{p,s}}{m_{nf}} \quad (6)$$

where c is the specific heat capacity, and m is the weight. The subscripts nf, np, and s designate the nanofluid, nanoparticle, and salt, respectively. The specific heat capacity of the base salt is 1.56 J/(g·K) as measured in the present work. According to the literature [43], the specific heat capacity of nanoparticles may exceed that of the corresponding bulk material by 15%. Using the bulk value of c_p = 0.97 J/(g·K) for SiO_2, that of SiO_2 nanoparticles is assumed to be 1.11 J/(g·K). According to equation (6), the specific heat capacity of the nanofluid should be lower than that of pure molten salt, while in the present work the former is up to ~8.4% higher than the latter. Thus, this model underestimates the effect of nanoparticles on the specific heat capacity of the nanofluid.

We also measured the specific heat capacity values of eutectic mixtures seeded with SiO_2 nanoparticles of different average sizes (10, 20, and 30 nm) as shown in Fig. 8, with their concentrations fixed at 1 wt.% according to the previous result. While the average specific heat capacity of the pure sample in liquid phase is about 1.56 J/(g·K), those seeded with nanoparticles 10, 20, and 30 nm in size are 1.691, 1.976, and 1.862 J/(g·K), respectively. In other words, the specific heat capacity enhancements of nanofluids with different nanoparticle sizes (10, 20 and 30 nm) were 8.4%, 26.7% and 19.4%, respectively. Therefore, the 20 nm nanoparticles produced the largest enhancement of specific heat capacity, almost up to 26.7% higher than that of pure salt. The measured specific heat capacities were listed in Table 3.

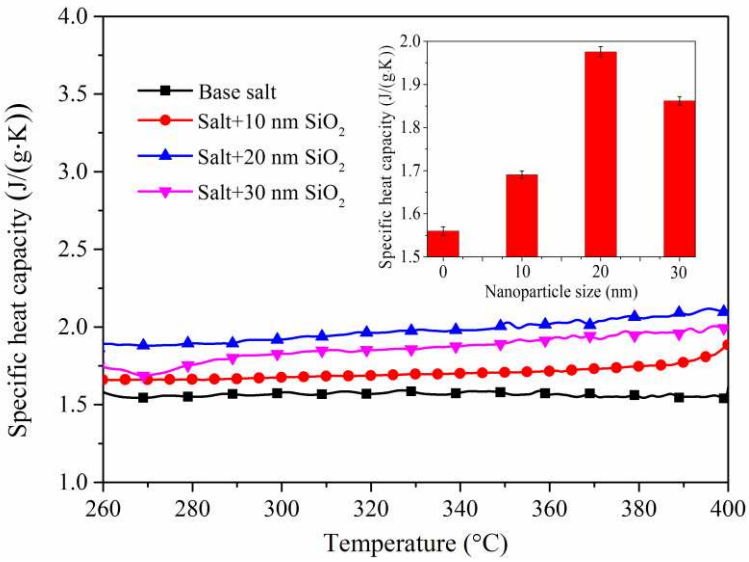

Fig. 8 Specific heat capacity vs. temperature for nanofluids with different size SiO_2 nanoparticles.

Table 3 Specific heat capacities of nanofluids with different nanoparticle sizes

Sample	Base salt	Salt+10 nm SiO_2	Salt+20 nm SiO_2	Salt+30 nm SiO_2
1# First	1.558	1.683	1.968	1.868
1# Second	1.570	1.689	1.964	1.871
1# Third	1.563	1.685	1.965	1.872
2# First	1.563	1.697	1.983	1.863
2# Second	1.555	1.699	1.988	1.862
2# Third	1.551	1.699	1.986	1.862
3# First	1.565	1.685	1.973	1.857
3# Second	1.552	1.690	1.98	1.853
3# Third	1.562	1.691	1.978	1.852
Average	1.560	1.691	1.976	1.862
Enhancement	--	8.4%	26.7%	19.4%

4.2 Material characterization

In general, the specific heat capacity of a material is related to its phase or structure. Hence, SEM was employed to examine the morphology of pure and nanofluid samples with different nanoparticle concentrations. From Fig. 9, the surface of the base salt is smooth and has little visible structures. Starting with Fig. 9 (a), little spots and blocks appear upon the addition of nanoparticles, and the amount of these structures increases with the nanoparticle concentration, as shown in Fig. 9 (b). According to the theory of Dudda and Shin [27], due to the temperature gradient between nanoparticles and surrounding molten salt molecules, there should be a concentration gradient of the binary salts from the surface of nanoparticle to away from the particle. Moreover, since the responding difference to the charge on the surface of nanoparticle, there will be a localized chemistry change. Combination of these effects, semi-solid layer forms on the surface of nanoparticle and grow away to formulate nanostructures. Upon further addition of nanoparticles, the amount of these small nanostructures is reduced, while some agglomeration appears (Fig. 9 (c) and (d)) possibly as a result of the reduced homogeneity. The chemical composition was determined by the energy dispersive X-ray spectroscopy (EDS) instrument attached to the SEM. Fig. 10 shows the EDS of O, Si, Na, and K elements in the sample containing 1.0 wt.% SiO_2 nanoparticles following the DSC measurement. Si has the same distribution as the other elements, indicating a uniform dispersion of Si in the

composite. No doubt, these small structures can significantly increase the specific surface area of the nanomaterials. It is believed that a thermal contact resistance exists at the interface between a liquid and a solid [44,45]. The interfacial thermal resistance acts as a thermal barrier. Jo and Banerjee thought thermal resistance was determined by a correlation considering the specific heat capacity, surface area and time constant of decaying particle temperature [34]. A high surface area will contribute to an anomalous increase in the interfacial thermal resistance between the solid phase and surrounding liquid molecules, thereby acting as additional thermal storage.

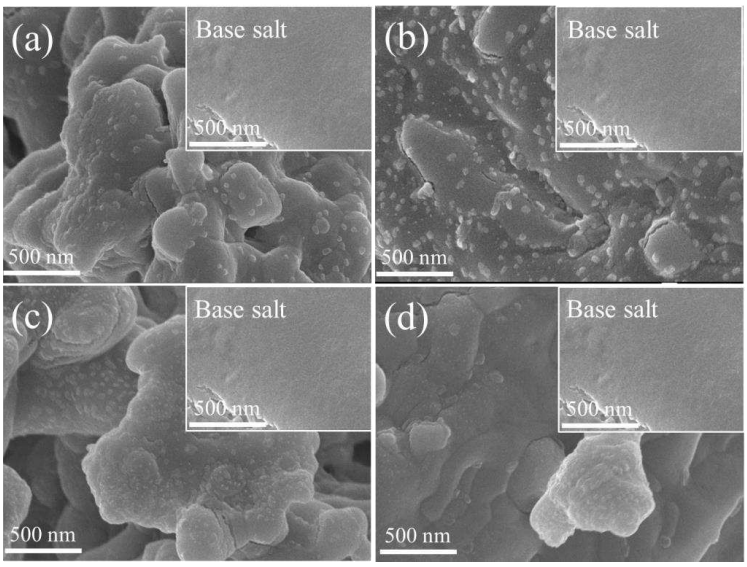

Fig. 9 SEM images of salt with various concentrations of nanoparticles after DSC measurement: (a) Salt+0.5 wt.% SiO_2, (b) Salt+1.0 wt.% SiO_2, (c) Salt+1.5 wt.% SiO_2, and (d) Salt+2.0 wt.% SiO_2.

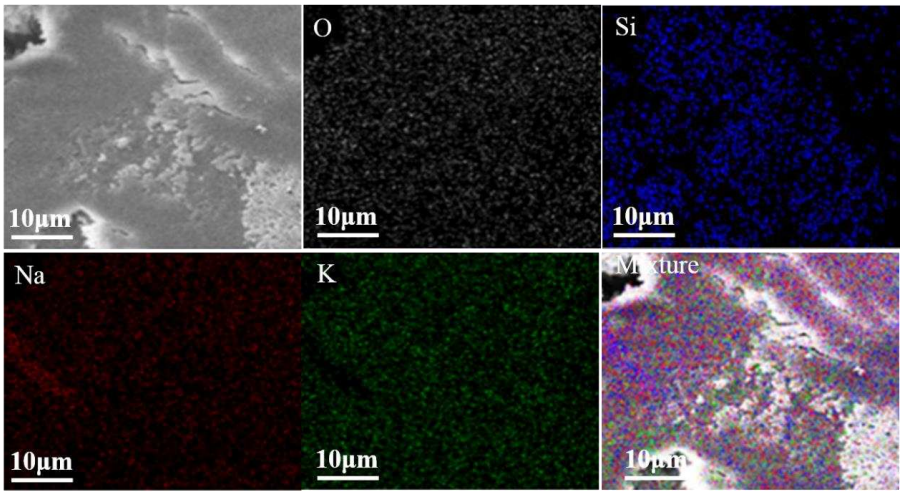

Fig. 10 EDS of the nanomaterial (1.0 wt.% SiO_2) after DSC measurement.

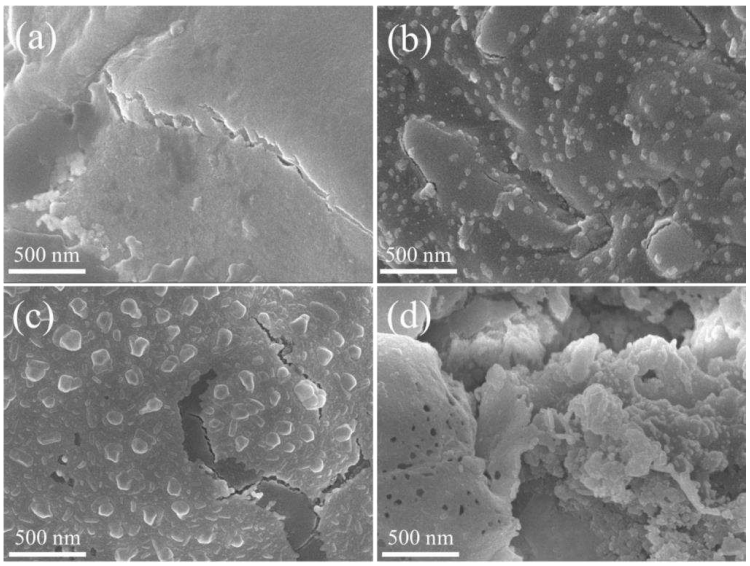

Fig. 11 SEM images of (a) Base salt, and with nanoparticles after DSC measurement: (b) Salt+10 nm SiO_2, (c) Salt+20 nm SiO_2, and (d) Salt+30 nm SiO_2 at 1.0 wt.% concentrations.

Fig. 11 shows the SEM images of the base salt and composites with 1.0 wt.% nanoparticles of various sizes (10, 20, and 30 nm) after the DSC measurement. Fig. 11 (a) shows the SEM image of pure molten salt. It can be seen that the surface is smooth. While in Fig. 11 (b), (c) and (d), some little spots and blocks appear. Comparing these three images, the sizes of little structures for salt with 10 nm nanoparticles are almost uniform while that for salt with 20 nm and 30 nm nanoparticles vary in a large range. The probable reason is that the surface charge for different size nanoparticle varies a lot, which induces different localized chemistry changes and forms different size of small structures. Afterwards, the small structures affect the specific heat capacity.

4.3 Molecular dynamics simulations

4.3.1 Density and specific heat capacity

To confirm that the potential and parameters used in the MD calculation are physical, the density and specific heat capacity of the molten salt were calculated for different nanoparticle mass concentrations. Fig. 12 compares the nanofluid density obtained from MD simulation and theoretical calculation, showing good agreement between the two. Usually, the density of a nanofluid is calculated using equation (7).

$$\rho_{\mathrm{nf}} = \varphi\rho_{\mathrm{p}} + (1-\varphi)\rho_{\mathrm{f}} \tag{7}$$

where φ is the volume fraction of nanoparticles; and subscripts p and f denote the nanoparticles and fluid, respectively.

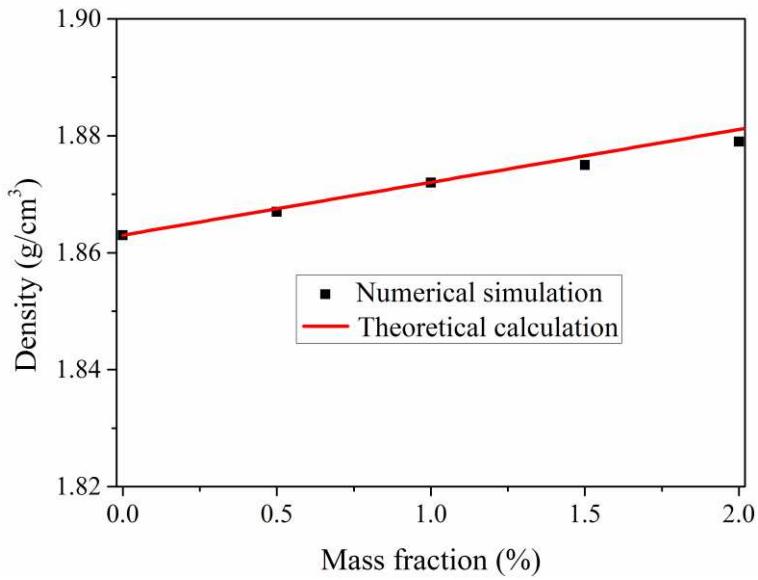

Fig. 12 Comparison of molten salt density from simulation and theoretical calculation.

Fig. 13 gives the relationship between the total energy of the ensemble and the temperature in 1.0 wt.% SiO_2-eutectic salt nanofluids. The total energy increases linearly with the temperature, with an Adj. R^2 = 0.99767. Therefore, the specific heat capacity of the SiO_2-molten salt nanofluid is almost constant in the temperature range of 550-750 K.

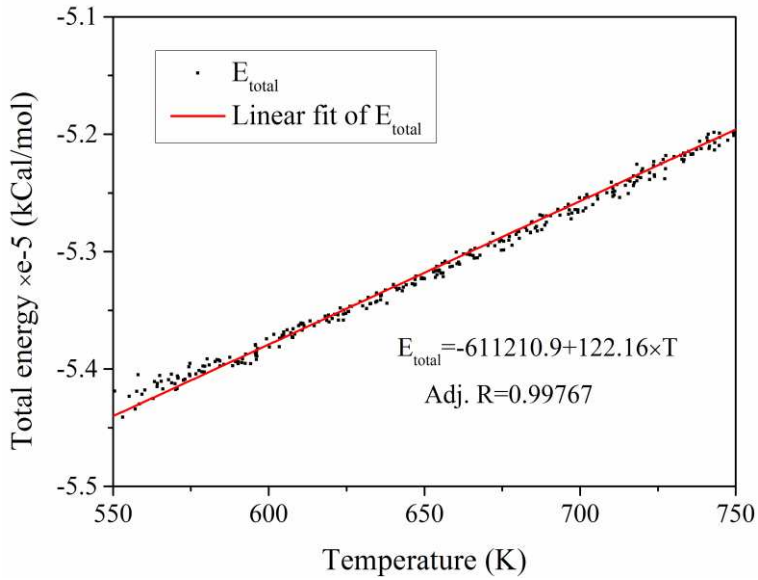

Fig. 13 Total energy of the ensemble versus temperature.

According to the MD results, specific heat capacity is calculated as follows:

$$c_p = \frac{\Delta E}{\Delta T \cdot V \cdot \rho} \tag{8}$$

where ΔE is the total energy change of the system after a temperature change of ΔT, V is the volume, and ρ is the density of the system. In Fig. 14, the experimental and

simulated specific heat capacity at different nanoparticle ratios shows the same trend: it first increases and then decreases with increasing nanoparticle mass concentration, with a maximum at 1.0 wt.%. Considering the much smaller nanoparticle size used in the simulation and the complex interaction between the nanoparticle and solvent molecules, the differences between the experimental and simulation results are considered acceptable.

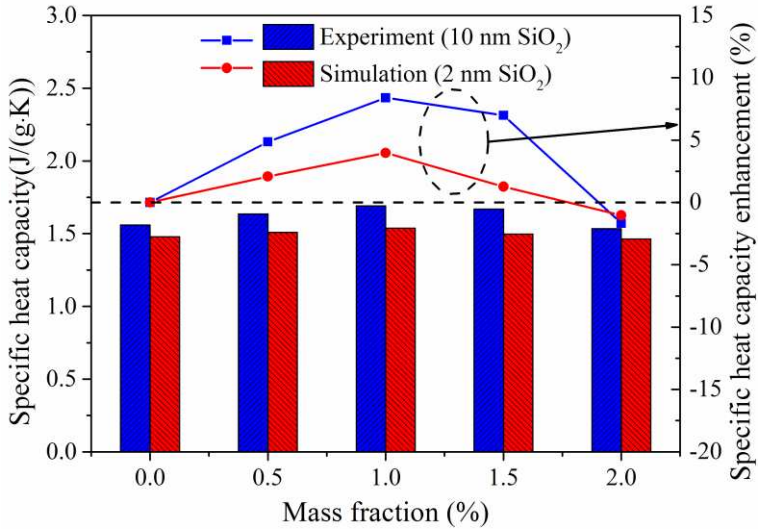

Fig. 14 Experimental and simulated specific heat capacity values with different nanoparticle mass concentrations in the salts.

4.3.2 Molecular-scale analysis

To further investigate the reason behind the enhanced specific heat capacity, we analyzed the different energy components for each atomic type from the simulation (Fig. 15). Since specific heat capacity is defined as the energy needed to raise the system temperature by 1 K, it is also a measurement of how much energy can be stored in the system. Equation (9) gives the expression of energy per atom, consisting of kinetic (E_{ke}) and potential (E_{pe}) parts.

$$E = E_{ke} + E_{pe} \tag{9}$$

The potential energy for each atom further consists of van der Waals, Coulombic, long-range Kspace, and molecular energy terms. From Fig. 15, there is no significant difference in the kinetic, molecular, and van der Waals energies for each atom, meaning that adding SiO_2 nanoparticles into the liquid molten salt has little effect on the movement and structure of the solvent molecules. The Coulombic energy, however, increases with the nanoparticle concentration up to 1.0 wt.%, after which it decreases. Meanwhile, the long-range Kspace energy decreases slightly with adding

more nanoparticles. Combining the effect on its four components, the total potential energy term increases with added silica nanoparticles up to 1.0 wt.% and then decreases at higher concentrations. Since the potential energy contributes more to the total system energy than the kinetic part, the specific heat capacity is mainly influenced by the potential energy change resulting from the changing Coulombic energy.

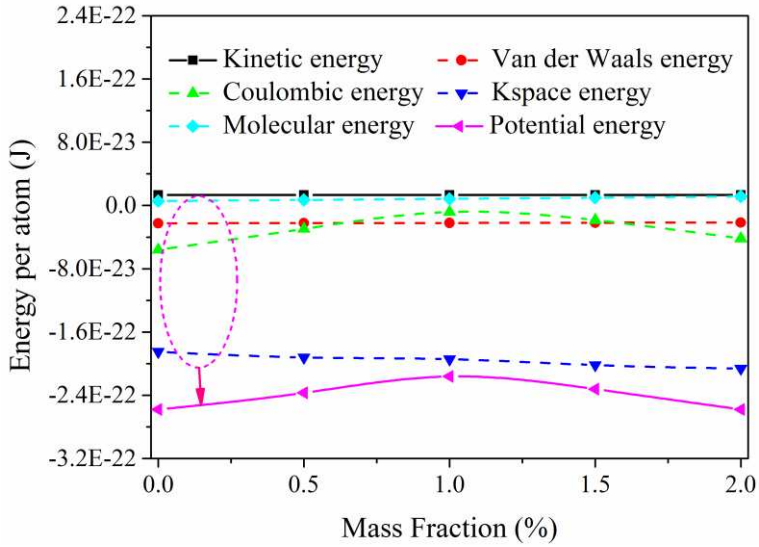

Fig. 15 Potential energy analysis of the nanofluid system at 650 K.

5. Conclusions

In this study, we investigated the influence of adding nanoparticles on the enhancement of specific heat capacity of molten salt. Composites with different amounts of nanoparticles (0.5–2.0 wt.%) were formulated, and their specific heat capacity values were measured by a DSC instrument. The results show that for 10 nm SiO_2 nanoparticles, the optimum concentration is 1.0 wt.% which corresponds to an 8.4% enhancement of specific heat capacity. Using this mass concentration, we further investigated the effect of the nanoparticle size. The average enhancements of specific heat capacity using 10, 20, and 30 nm nanoparticles in the liquid phase were found to be 8.4%, 26.7%, and 19.4%, respectively. Therefore, the effect of nanoparticle size on specific heat capacity is not monotonous.

The material characteristics indicate that specific heat capacity of nanofluids increases with the number of formed nanostructures, which significantly augment the surface area of the nanomaterial, leading to a higher contribution of surface energy to the effective heat capacity. According to the MD simulation results, adding

nanoparticles into molten salt mainly changes the Coulombic energy of each atom to influence the specific heat capacity of the system. The nanofluids with 1.0 wt.% nanoparticles show the largest potential energy enhancement (i.e., the highest specific heat capacity), in accordance with the experimental observations. Therefore, such MD simulations can help people understand the internal interaction between nanoparticles and molten salt molecules.

Acknowledgements

This work is financially supported by the Science Creative Foundation for Distinguished Young Scholars in Heilongjiang (Grant No. JC2016009), the Science Creative Foundation for Distinguished Young Scholars in Harbin (Grant No. 2014RFYXJ004) and the Fundamental Research Funds for the Central Universities (Grant No. HIT. BRETIV. 201315).

Reference

[1]. K. Pielichowska, K. Pielichowski, Phase change materials for thermal energy storage, Prog. Mater. Sci. 65 (2014) 67–123. doi:10.1016/j.pmatsci.2014.03.005.

[2]. Y. Tian, C.Y. Zhao, A review of solar collectors and thermal energy storage in solar thermal applications, Appl. Energy. 104 (2013) 538–553. doi:10.1016/j.apenergy.2012.11.051.

[3]. H.L. Zhang, J. Baeyens, J. Degrève, G. Cacères, Concentrated solar power plants: Review and design methodology, Renew. Sustain. Energy Rev. 22 (2013) 466–481. doi:10.1016/j.rser.2013.01.032.

[4]. H. Zhang, J. Baeyens, G. Cáceres, J. Degrève, Y. Lv, Thermal energy storage: Recent developments and practical aspects, Prog. Energy Combust. Sci. 53 (2016) 1–40. doi:10.1016/j.pecs.2015.10.003.

[5]. C. Yang, M.E. Navarro, B. Zhao, G. Leng, G. Xu, L. Wang, Y. Jin, Y. Ding, Thermal conductivity enhancement of recycled high density polyethylene as a storage media for latent heat thermal energy storage, Sol. Energy Mater. Sol. Cells. 152 (2016) 103–110. doi:10.1016/j.solmat.2016.02.022.

[6]. V.M.B. Nunes, C.S. Queirós, M.J. V Lourenço, F.J. V Santos, C.A. Nieto de Castro, Molten salts as engineering fluids-A review: Part I. Molten alkali nitrates, Appl. Energy. 183 (2016) 603–611. doi:10.1016/j.apenergy.2016.09.003.

[7]. Y. Wu, Y. Li, Y. Lu, H. Wang, C. Ma, Novel low melting point binary nitrates for thermal energy storage applications, Sol. Energy Mater. Sol. Cells. 164 (2017) 114–121. doi:10.1016/j.solmat.2017.02.021.

[8]. S.U.S. Choi, J.A. Eastman, Enhancing thermal conductivity of fluids with nanoparticles, in: ASME Int. Mech. Eng. Congr. Expo., 1995: pp. 99–105. doi:10.1115/1.1532008.

[9]. D. Wen, Y. Ding, Experimental investigation into convective heat transfer of nanofluids at the entrance region under laminar flow conditions, Int. J. Heat Mass Transf. 47 (2004) 5181–5188.

doi:10.1016/j.ijheatmasstransfer.2004.07.012.
[10]. S.M.S. Murshed, C.A. Nieto de Castro, Conduction and convection heat transfer characteristics of ethylene glycol based nanofluids – A review, Appl. Energy. 184 (2016) 681–695. doi:10.1016/j.apenergy.2016.11.017.
[11]. R.S. Vajjha, D.K. Das, Experimental determination of thermal conductivity of three nanofluids and development of new correlations, Int. J. Heat Mass Transf. 52 (2009) 4675–4682. doi:10.1016/j.ijheatmasstransfer.2009.06.027.
[12]. R. Ni, S.Q. Zhou, K.Q. Xia, An experimental investigation of turbulent thermal convection in water-based alumina nanofluid, Phys. Fluids. 23 (2011). doi:10.1063/1.3553281.
[13]. R. Hentschke, On the specific heat capacity enhancement in nanofluids, Nanoscale Res. Lett. 11 (2016) 88. doi:10.1186/s11671-015-1188-5.
[14]. D. Shin, D. Banerjee, Enhanced Specific Heat of Silica Nanofluid, J. Heat Transfer. 133 (2011) 24501. doi:10.1115/1.4002600.
[15]. D. Shin, D. Banerjee, Enhancement of specific heat capacity of high-temperature silica-nanofluids synthesized in alkali chloride salt eutectics for solar thermal-energy storage applications, Int. J. Heat Mass Transf. 54 (2011) 1064–1070. doi:10.1016/j.ijheatmasstransfer.2010.11.017.
[16]. Y.B. Tao, C.H. Lin, Y.L. He, Preparation and thermal properties characterization of carbonate salt/carbon nanomaterial composite phase change material, Energy Convers. Manag. 97 (2015) 103–110. doi:10.1016/j.enconman.2015.03.051.
[17]. X. Chen, Y. ting Wu, L. di Zhang, X. Wang, C. fang Ma, Experimental study on the specific heat and stability of molten salt nanofluids prepared by high-temperature melting, Sol. Energy Mater. Sol. Cells. 176 (2018) 42–48. doi:10.1016/j.solmat.2017.11.021.
[18]. Y. Luo, X. Du, A. Awad, D. Wen, Thermal energy storage enhancement of a binary molten salt via in-situ produced nanoparticles, Int. J. Heat Mass Transf. 104 (2017) 658–664. doi:10.1016/j.ijheatmasstransfer.2016.09.004.
[19]. M. Lasfargues, Q. Geng, H. Cao, Y. Ding, Mechanical Dispersion of Nanoparticles and Its Effect on the Specific Heat Capacity of Impure Binary Nitrate Salt Mixtures, Nanomaterials. 5 (2015) 1136–1146. doi:10.3390/nano5031136.
[20]. L. Zhang, X. Chen, Y. Wu, Y. Lu, C. Ma, Effect of nanoparticle dispersion on enhancing the specific heat capacity of quaternary nitrate for solar thermal energy storage application, Sol. Energy Mater. Sol. Cells. 157 (2016) 808–813. doi:10.1016/j.solmat.2016.07.046.
[21]. B. Jo, D. Banerjee, Enhanced specific heat capacity of molten salt-based nanomaterials: Effects of nanoparticle dispersion and solvent material, Acta Mater. 75 (2014) 80–91. doi:10.1016/j.actamat.2014.05.005.
[22]. B. Jo, D. Banerjee, Effect of Dispersion Homogeneity on Specific Heat Capacity Enhancement of Molten Salt Nanomaterials Using Carbon Nanotubes, J. Sol. Energy Eng. 137 (2014) 11011. doi:10.1115/1.4028144.
[23]. M.X. Ho, C. Pan, Optimal concentration of alumina nanoparticles in molten Hitec salt to maximize its specific heat capacity, Int. J. Heat Mass Transf. 70 (2014) 174–184. doi:10.1016/j.ijheatmasstransfer.2013.10.078.
[24]. L. Sang, T. Liu, The enhanced specific heat capacity of ternary carbonates nanofluids with different nanoparticles, Sol. Energy Mater. Sol. Cells. 169 (2017) 297–303. doi:10.1016/j.solmat.2017.05.032.
[25]. J. Seo, D. Shin, Size effect of nanoparticle on specific heat in a ternary nitrate

($LiNO_3$-$NaNO_3$-KNO_3) salt eutectic for thermal energy storage, Appl. Therm. Eng. 102 (2016) 144–148. doi:10.1016/j.applthermaleng.2016.03.134.

[26]. H. Tiznobaik, D. Shin, Enhanced specific heat capacity of high-temperature molten salt-based nanofluids, Int. J. Heat Mass Transf. 57 (2013) 542–548. doi:10.1016/j.ijheatmasstransfer.2012.10.062.

[27]. B. Dudda, D. Shin, Effect of nanoparticle dispersion on specific heat capacity of a binary nitrate salt eutectic for concentrated solar power applications, Int. J. Therm. Sci. 69 (2013) 37–42. doi:10.1016/j.ijthermalsci.2013.02.003.

[28]. D. Shin, D. Banerjee, Enhanced Specific Heat Capacity of Nanomaterials Synthesized by Dispersing Silica Nanoparticles in Eutectic Mixtures, J. Heat Transfer. 135 (2013) 32801. doi:10.1115/1.4005163.

[29]. D. Shin, D. Banerjee, Enhanced thermal properties of SiO_2 nanocomposite for solar thermal energy storage applications, Int. J. Heat Mass Transf. 84 (2015) 898–902. doi:10.1016/j.ijheatmasstransfer.2015.01.100.

[30]. H. Riazi, S. Mesgari, N.A. Ahmed, R.A. Taylor, The effect of nanoparticle morphology on the specific heat of nanosalts, Int. J. Heat Mass Transf. 94 (2016) 254–261. doi:10.1016/j.ijheatmasstransfer.2015.11.064.

[31]. X. Chen, A. Munjiza, K. Zhang, D. Wen, Molecular Dynamics Simulation of Heat Transfer from a Gold Nanoparticle to a Water Pool, J. Phys. Chem. C. 118 (2014) 1285–1293. doi:10.1021/jp410054j.

[32]. G. Nagayama, P. Cheng, Effects of interface wettability on microscale flow by molecular dynamics simulation, Int. J. Heat Mass Transf. 47 (2004) 501–513. doi:10.1016/j.ijheatmasstransfer.2003.07.013.

[33]. G. Qiao, M. Lasfargues, A. Alexiadis, Y. Ding, Simulation and experimental study of the specific heat capacity of molten salt based nanofluids, Appl. Therm. Eng. 111 (2017) 1517–1522. doi:10.1016/j.applthermaleng.2016.07.159.

[34]. B. Jo, D. Banerjee, Interfacial Thermal Resistance Between a Carbon Nanoparticle and Molten Salt Eutectic : Effect of Material Properties , Particle shapes and sizes, in: Proc. ASME/JSME 8th Therm. Eng. Jt. Conf., American Society of Mechanical Engineers, Honolulu, 2011: pp. 1–7.

[35]. B. Jo, D. Banerjee, Effect of solvent on specific heat capacity enhancement of binary molten salt-based carbon nanotube nanomaterials for thermal energy storage, Int. J. Therm. Sci. 98 (2015) 219–227. doi:10.1016/j.ijthermalsci.2015.07.020.

[36]. ASTM E1269-11, Standard Test Method for Determining Specific Heat Capacity by Differential Scanning, Am. Soc. Test. Mater. (2011) 1–6. doi:10.1520/E1269-11.2.

[37]. M. Palmer, Propagation of Uncertainty through Mathematical Operations, MIT Modul. (2003) 1–7.

[38]. B. Jo, D. Banerjee, Molecular dynamics study on interfacial thermal resistance between organic nanoparticles and alkali molten salt mixtures, Int. J. Multiscale Comput. Eng. 15 (2017) 199–217. doi:10.1615/IntJMultCompEng.2017018709.

[39]. L. Li, Y. Zhang, H. Ma, M. Yang, An investigation of molecular layering at the liquid-solid interface in nanofluids by molecular dynamics simulation, Phys. Lett. A. 372 (2008) 4541–4544. doi:10.1016/j.physleta.2008.04.046.

[40]. S. Jayaraman, A.P. Thompson, O.A. von Lilienfeld, E.J. Maginn, Molecular Simulation of the Thermal and Transport Properties of Three Alkali Nitrate Salts, Ind. Eng. Chem. Res. 49 (2010)

559–571. doi:10.1021/ie9007216.
[41]. M.R. Betts, The effects of nanoparticle augmentation of nitrate thermal storage materials for use in concentrating solar power applications, A Thesis Master Sci. (2011).
[42]. N.J. Bridges, A.E. Visser, E.B. Fox, Potential of Nanoparticle-Enhanced Ionic Liquids (NEILs) as Advanced Heat-Transfer Fluids, Energy & Fuels. 25 (2011) 4862–4864. doi:10.1021/ef2012084.
[43]. L. Wang, Z. Tan, S. Meng, D. Liang, G. Li, Enhancement of molar heat capacity of nanostructured Al_2O_3, J. Nanoparticle Res. 3 (2001) 483–487. doi:10.1023/A:1012514216429.
[44]. R.J. Warzoha, A.S. Fleischer, Heat flow at nanoparticle interfaces, Nano Energy. 6 (2014) 137–158. doi:10.1016/j.nanoen.2014.03.014.
[45]. M. Zain-ul-abdein, K. Raza, F.A. Khalid, T. Mabrouki, Numerical investigation of the effect of interfacial thermal resistance upon the thermal conductivity of copper/diamond composites, Mater. Des. 86 (2015) 248–258. doi:10.1016/j.matdes.2015.07.059.